Shahrood University of Technology
Iranian Society of Mining Engineering (IRSME)
Journal of Mining and Environment (JME)
journal homepage: www.jme.shahroodut.ac.ir
THOMSON REUTERS
Vol. 10, No. 3, 2019, 575-595.
DOI: 10.22044/jme.2018.7104.1558

Delineation of alteration zones based on kriging, artificial neural networks, and concentration–volume fractal modelings in hypogene zone of Miduk porphyry copper deposit, SE Iran

O. Gholampour[1], A. Hezarkhani[1*], A. Maghsoudi[1] and M. Mousavi[2]

1. Department of Mining and Metallurgy Engineering, Amirkabir University of technology (Tehran Polytechnic), Tehran, Iran
2. National Iranian Copper Industries Company, Miduk Mine, Kerman, Iran

Received 26 May 2018; received in revised form 18 July 2018; accepted 21 July 2018

Keywords

Concentration–Volume (C–V) Fractal Model

Ordinary Kriging (OK)

Artificial Neural Networks (ANNs)

Miduk Porphyry Copper Deposit

Alteration Zones

Abstract

This paper presents a quantitative modeling for delineating alteration zones in the hypogene zone of the Miduk porphyry copper deposit (SE Iran) based on the core drilling data. The main goal of this work was to apply the Ordinary Kriging (OK), Artificial Neural Networks (ANNs), and Concentration-Volume (C-V) fractal modelings on Cu grades to separate different alteration zones. Anisotropy was investigated and modeled based on calculating the experimental semi-variograms of Cu value, and then the main variography directions were identified and evaluated. The block model of Cu grade was generated using the kriging and ANN modelings followed by log-log plots of the C-V fractal modeling to determine the Cu threshold values used in delineating the alteration zones. Based on the correlation between the geological models and the results derived via C-V fractal modeling, Cu values less than 0.479% resulting from kriging modeling had more overlapped voxels with the phyllic alteration zone by an overall accuracy (OA) of 0.83. The spatial correlation between the potassic alteration zone in a 3D geological model and the high concentration zones in the C-V fractal model showed that Cu values between 0.479% and 1.023%, resulting from kriging modeling, had the best overall accuracy (0.78). Finally, based on the correlation between classes in the binary geological and fractal models of the hypogene zone, this research work showed that kriging modeling could delineate the phyllic (with lower grades) and potassic (with higher grades) alteration zones more effectively compared with ANNs.

1. Introduction

The knowledge of ore grades, for example Cu grade, is vital information and one of the most complicated aspects of both mineral exploration and mining. On the other hand, ore grade information is a foundation for ore grade control, ore reserve evaluation, mine valuation, pit optimization, and production scheduling [1, 2]. Multiple factors affect an ore grade model including the complexity and the spatial continuity of the ore body, adequacy of the data to monitor the spatial variability, and types of techniques used [3].

In the past few decades, many attempts have been made to achieve a reliable model of ore grades. At the beginning, the conventional methods such as core drilling combined with chemical analysis would apply to achieve an ore grade model. However, too much core drilling without considering the spatial dependency is expensive and time-consuming. Therefore, geostatistical techniques were introduced, which were based upon spatial relationships between the sample locations and the sample components in space. Also the underlying assumption of geostatistics (mean and covariance) is stationary [4-6].

The geostatistical methodology begins with two

Corresponding author: ardehez@aut.ac.ir (A. Hezarkhani).

major steps: structural analysis and kriging. Over the past 50 years, many researchers have used various geostatistical methods such as simple kriging, Ordinary Kriging (OK), lognormal kriging, indicator kriging, co-kriging, universal kriging, residual kriging, moving window regression residual kriging, disjunctive kriging, and stochastic simulation such as Sequential Gaussian Simulation (SGS) and Sequential Indicator Simulation (SIS) in ore grade modeling. Kriging, as a group of geostatistical methods, is an interpolation technique that considers both the degree of variation and the distance between known data points in estimating the values in unknown areas [7-18].

Despite the widespread application of geostatistical methods, they suffer from some limitations. They are based upon certain stationary assumptions like being a second-order stationary random field with an unknown constant mean as well as using a linear correlation between any two points in space and applying the variogram model for representing a complex geological setting. Furthermore, the algorithm requires abundant data to be processed, which restricts their learning and efficient application. Other disadvantages of this method include requiring deep mathematical thinking and skills and taking too much time to get the preferred solution [4, 14, 19].

Due to the aforementioned problems, many research works have been conducted to inspire from nature. One of the methods inspired from nature is computational intelligent methods including neural networks (NNs), evolutionary computation (EC), swarm intelligence (SI), and fuzzy systems (FS) [20-27]. An alternative approach that has been considered particularly in the last decade for grade estimation is the application of Artificial Neural Networks (ANNs) systems. Neural networks have emerged as powerful tools to model complex systems [28]. The NN analysis enables the estimation of ore grades using various algorithms with sparse analog data as the input. Since the data analytical approaches are carried out in parallel and distributed methods in neural networks, their ability to recognize the complex relationships between multiple variables can be presented to NN. In general, the purposes of ANNs applied to grade estimation include (a) a fast and reliable grade estimation, (b) minimizing the required assumptions on grade distribution, (c) minimizing expert knowledge requirements, and (d) making the quality of the estimates independent from the skills and knowledge of the expert [19, 29, 30]. However, there are several problems concerning the efficiency of NNs that affect their performance like the topology, weight, and training parameters [31].

Identification of geological units using petro-graphical and mineralogical studies and borehole data is performed by applying different conventional methods, which discretize different populations but ore grades are not considered in all of the resulting models. The relationship between the geological variation and ore grades leads to using another data processing approach like fractal geometry that describes the complexity in data distribution to find different geological units [32, 33].

Natural phenomena like geo-related sciences cannot be investigated through Euclidean geometry [34]. Mandelbrot (1983) has proposed the fractal geometry, which can explain natural processes [35]. Fractal/multi-fractal modeling, as a useful data processing method, can be applied on geosciences like geochemical exploration, mineral exploration, and economic geology [36-46].

The complex spatial distribution of ore elements has fractal dimensions, which shows a self-similarity in different geographical scales. Differences in some of the physical characteristics in geological and geochemical processes such as vein density or orientation, lithology, fluid phase, structural feature, alteration phenomena, and dominant mineralogy correspond to fractal dimensions, so it is possible to find the geological populations and the corresponding spatial models. Threshold values in fractal/multi-fractal log-log plots may be used to discriminate different populations such as various types of alterations and mineralized or barren zones [32, 41, 43, 47-55].

During the recent decades, various fractal methods have been proposed in different branches of geosciences, especially geochemical pattern recognition such as Number-Size [35], Concentration-Area [38], Size-Grade [37], Concentration-Perimeter [56], Spectrum-Area [57], Concentration-Distance [42], Concentration-Volume [32], Spectrum-Volume [58], Concentration-Number [41], and Simulated Size-Number [59].

In this paper, we aimed to compare the abilities of the ANNs and kriging methods for estimating the block model of ore grades in order to determine the best model in isolating the societies under the C-V fractal process, and finally, to give the best alteration model in the hypogene zone of the

Miduk mine. The efficacy of the models was measured in comparison with the geological logging information, and their performance was compared with each other.

This paper is organized as what follow. In the next two sections, various aspects of regional geology, geological setting, and alteration zones of the studied area are investigated. Section 4 gives an overview of the methods, and their principles, advantages, and limitations. The results obtained are discussed in Section 5. Finally, the conclusions are presented in Section 6.

2. Geological setting

Among the copper deposits, porphyry deposits are the world main copper resources that supply three-fourths of the world copper production [60]. Various compositions and igneous rocks host porphyry copper deposits (PCDs). Granodiorite, quartz monzonite, quartz diorite, diorite, monzonite, andesite, and dacite are the most important host rocks of PCDs. These diverse rock types host different world-class deposits like Butte, Montana (Quartz monzonite), Cananea, Mexico (granodiorite), Caspiche, Chile (diorite), and Miduk, Iran (quartz diorite) [61-64].

Most PCDs in Iran occur in the Cenozoic Sahand-Bazman orogenic belt (Figure 1), which has been introduced by the subduction of the Arabian plate under the central Iran during the Alpine orogeny [65-67]. The most important copper deposits of Iran (e.g. Miduk, Sar-Cheshmeh, and Sungun) occur in this orogenic belt in association with mid- to late-Miocene diorite/granodiorite to quartz-monzonite stocks [20, 26, 68-71].

The Miduk porphyry copper deposit is located in the Shahr-Babak area (Kerman province, Iran), 85 km NW of the Sar-Cheshmeh PCD. The deposit was explored in 1970s after the exploration of the Sar-Cheshmeh deposit. The Miduk deposit is surrounded by intensely biotitized volcanic rocks and is hosted by a quartz diorite stock [20, 72, 73].

3. Mineralization and alteration

Alteration, mineralization, and distribution of veins in different world PCDs show similar patterns [63, 74-76]. The typical alteration zonation comprises the inner potassic alteration (K-silicates), sericitic alteration (that may cut the K-silicate zone), and the outer propylitic alteration [77, 78]. Investigations on the Miduk PCD show that the alterations are formed in an alkali metasomatic process, and include potassic, transitional (potassic-sodic), phyllic, and propylitic. The dominant alterations in the initial hydrothermal process are potassic and propylitic, followed by a later phyllic alteration [20, 26, 79, 80].

3.1. Potassic alteration zone

The potassic alteration zone of the Miduk PCD is the first intense alteration zone that is characterized by potassic minerals like K-feldspar, Mg-enriched biotite, and anhydrite. This zone was formed during the alkali metasomatism developed as halos surrounding the veins mostly in the deep and central parts of the Miduk stock. There is a close spatial relationship between the potassic alteration and mineralization, in which 70% of the copper content was emplaced [20].

3.2. Propylitic alteration zone

Ubiquitous epidote, chlorite (± pyrite ± calcite), and plagioclase crystals are the main observed minerals in this 400-meter-wide alteration zone. The propylitic alteration zone has a relatively sharp border with the potassic alteration zone in depth but the border is cut by the later phyllic zone at shallow levels. Chloritization of biotite crystals (primary and secondary) and groundmass in the rocks around the central potassic zone represent the propylitic alteration [20].

3.3. Sodic alteration zone

In the central part of the stock, the potassic zone was overprinted by the pervasive sodic alteration that changed peripherally into the phyllic alteration. Albite rims on orthoclase, albite replacement of An-rich plagioclase, and the distinct white color of the altered rocks are some of the characteristics of this alteration [20].

3.4. Phyllic alteration zone

An increase in the muscovite proportion causes a gradual change, which transits the sodic alteration to the phyllic alteration. Separation of the phyllic and sodic alteration zones is not easy due to the intense silicification caused by the latter alteration process. During this weak alteration, the reserve is overprinted by alkali metasomatic assemblages and contains pyrite ± chalcopyrite ± quartz veins. The replacement of rock-forming silicates by sericite and quartz is another characteristic of the phyllic alteration [20].

3.5. Argillic alteration zone

In this alteration, the partial alteration of feldspar to clay minerals occurs down to a depth of 20 m and an assemblage of clay minerals, quartz, and hematite replaces the entire rock. The dominant

phyllosilicate mineral is kaolinite, which is accompanied by illite [20].

3.6. Supergene enrichment

There are two different mineralized zones in the supergene enrichment phase of the Miduk PCD containing the leached oxidized and the supergene sulfide zones. The leached capping layer, which covers the supergene sulfide blanket, is 50 m thick in average and contains limonite, copper carbonates, and chalcanthite. Moreover, the supergene zone is several meters thick, and principally contains chalcocite with a minor amount of covellite [20].

3.7. Hypogene zone

Copper mineralization in the hypogene zone of the Miduk PCD seems to be introduced during the transition from the potassic/sodic to the phyllic alteration. The predominant occurrence of earlier mineralization is in veins with sercitic halos in the potassic zone, and the later mineralization occurs mainly as disseminations and veinlets. The main copper mineralization during the potassic alteration consists of chalcopyrite and minor bornite, while the later phase of the hypogene mineralization only includes chalcopyrite. Sericitization and chloritization of feldspars and biotite occur from the central part of the stock to the margins, and are accompanied by an increase in the sulfide content. From the richest hypogene copper mineralization zone to the margins, the ratio of pyrite to chalcopyrite varies from 3:1 to 13:1 [20].

4. Methods

4.1. Ordinary kriging (OK)

Over the past decades, different spatial interpolation methods have been presented by numerous researchers. However, most of them are related together and have similar principles. Spatial interpolation models can be categorized into two classes: (a) mechanical/deterministic, and (b) statistical/probability groups. The mechanical models are based upon empirical model parameters, which include techniques like Inverse Distance Weighting (IDW) and Splines. They do not consider the error estimation. In contrast, the parameters of statistical/probability techniques are estimated based on the probability principals and consider the error estimation. One of the most important statistical/probability models is kriging, which is based on the "Theory of Regionalized Variables" [81, 82]. The technique was first introduced by Krige (1951) but in 1963, G. Matheron derived the formulas and founded the linear geostatistics [83, 84]. The kriging technique, which is commonly known as a 'minimum variance estimator', consists of two basic steps. The first is an estimation of the semi-variogram using sample data, given by:

$$\gamma(h)=\frac{1}{2.n(h)}\sum_{i=1}^{n(h)}\{z(i)-z(i+h)\}^2 \quad (1)$$

where $\gamma(h)$ is the estimate of semi-variance, n(h) is the number of pairs observed [z(i), z(i+h)], and h is the distance between the pairs.

The second is predicting the value at unknown spatial coordinates through a linear combination of measured values shown by:

$$z^*(x_0)=\sum_{i=1}^{n}\lambda_i.z(x_i) \quad (2)$$

where $z^*(x_0)$ is the estimated value for any location x_0, n is the number of measured value z(i), $z(x_i)$ is the value involved in the estimation, and λ_i is the weight attached to each measured value z(i).

The best estimator is always unbiased and has a minimum variance. Therefore, the kriging system can be deduced as:

$$\sum_{j=1}^{n}\lambda_j.\gamma(x_i,x_j)=\mu+\gamma(x_i,x_0) \quad (3)$$

where $\gamma(x_i,x_0)$ is the semi-variance function of a vector with an origin at xi and extremity at x_0; $\gamma(x_i,x_j)$ is the semi-variance function of a vector with an origin at x_i and extremity at x_j; and μ is the Lagrangian multiplier [82].

OK is an appropriate geostatistical estimator and the most useful technique among the different kriging methods [4, 82, 85]. OK, as a linear estimation method, assigns weights to the sample locations inside the estimation neighborhood, which are independent from the data values at these locations. OK is a moving average method satisfying the different types of data dispersion, e.g. sparse sampling points [32, 86-88]. The technique minimizes the conditional bias and estimation variance for each single estimate at each location [13, 84, 89]. Most of the theories about OK relies on the work of Georges Matheron (1963), and have been developed by some others [4, 90-94].

In mathematical terms, OK is a spatial interpolation estimator $\hat{Z}(x_0)$ that is used to find

the best linear unbiased estimate of a second-order stationary random field with an unknown constant mean, as follows:

$$\hat{Z}(x_0) = \sum_{i=1}^{n} \lambda_i Z(x_i) \quad (4)$$

where $\hat{Z}(x_0)$ = kriging estimate at a non-sampled location x_0; $Z(x_0)$ = sampled value at location x_i; and λ_i = weighting factor for $Z(x_i)$.
The estimation error is:

$$\hat{Z}(x_0) - Z(x_0) = R(x_0) = \sum_{i=1}^{N} \lambda_i Z(x_i) - Z(x_0) \quad (5)$$

where $Z(x_0)$ = unknown true value at x_0; and $R(x_0)$ = estimation error. For an unbiased estimator, the mean of the estimation error must equal zero. Therefore:

$$E\{R(x_0)\} = 0 \quad (6)$$

And

$$\sum_{i=1}^{N} \lambda_i = 1 \quad (7)$$

A minimum variance of estimation error is required for solving the interpolation problem by kriging [85-87, 92, 93].

4.2. Artificial neural networks (ANNs)

A very powerful method that has attracted the attention of the researchers over the past few decades is ANNs, which has been used for ore grade modeling [31]. ANNs has a non-linear mathematical structure that is able to perform any curve-fitting operation in a multi-dimensional space. Hence, it is able to represent an arbitrarily complex data generating a process that links the inputs and outputs of that process [95].
In ore grade modeling/estimation, it is supposed that the attributed grade value in an ore deposit varies from one location to another, and this will be reflected in a complex input and output spatial relationship between grade values and spatial coordinates in the area of interest. Therefore, the output grade is considered to be a function of spatial coordinates like X, Y, and Z [96, 97].
There are many artificial neural network types such as feed forward neural network, Radial Basis Function (RBF) network, and Kohonen self-organizing network [98]. Three major components are particularly important in every ANN system: (a) structure of the nodes, (b) topology of the network, and (c) the learning algorithm used to find the weights of the ANNs. On the other hand, in an ANN, each processing unit acts as an idealized neuron, receives input, computes activation, and transmits that activation to other processing units. A weight value, defined to represent the connection strength, is associated with each connection between these processing units. The connection weight of each processing unit is optimally determined through the presentation of known examples, and application of a learning rule. Once the connection weight is determined through NN learning, the inter-connection between input and output embedded in the data is captured [99].
An architecture of ANNs with a sigmoid activation function is presented in Figure 2. It contains an input layer, a hidden layer, and one output layer, which are connected by modifiable weights and represented by links between the layers. Each input vector is presented as the input layer, and the output of each input unit equals the corresponding elements in the vector. Each hidden unit computes the weighted sum of its input to form its net activation [100]. The above-mentioned subjects can be expressed in mathematical terms by Eq. (8):

$$net_j = \sum_{i=1}^{d} x_i w_{ij} + w_{j0} = \sum_{i=0}^{d} x_i w_{ij} \quad (8)$$

where the subscripts i and j are indexed units in the input and hidden layers, respectively, W_{ij} denotes the input to the hidden layer weights at the hidden unit j, and net_j is the activation for hidden j.
Each hidden unit emits an output that is a non-linear function of its activation, f(net), in the form of Eq. (9):

$$y_j = f(net_j) \quad (9)$$

Each output unit similarly computes its net activation based on the hidden unit signals as Eq. (10):

$$net_k = \sum_{j=1}^{n_H} y_j w_{kj} + w_{k0} = \sum_{j=0}^{n_H} y_j w_{kj} \quad (10)$$

where the subscript k indexes the units in the output layer and n_H denotes the number of hidden units. An output unit computes the non-linear function of its net, as Eq. (11):

$$z_k = f(net_k) \quad (11)$$

where z_k is the k output unit. Therefore, the total network output for a three-layer model can be calculated in the form of Eq. (12) [96]:

$$z_k = f\left(\sum_{j=1}^{n_H} w_{kj} f\left(\sum_{i=1}^{d} w_{ji} x_i + w_{j0}\right) + w_{k0}\right) \quad (12)$$

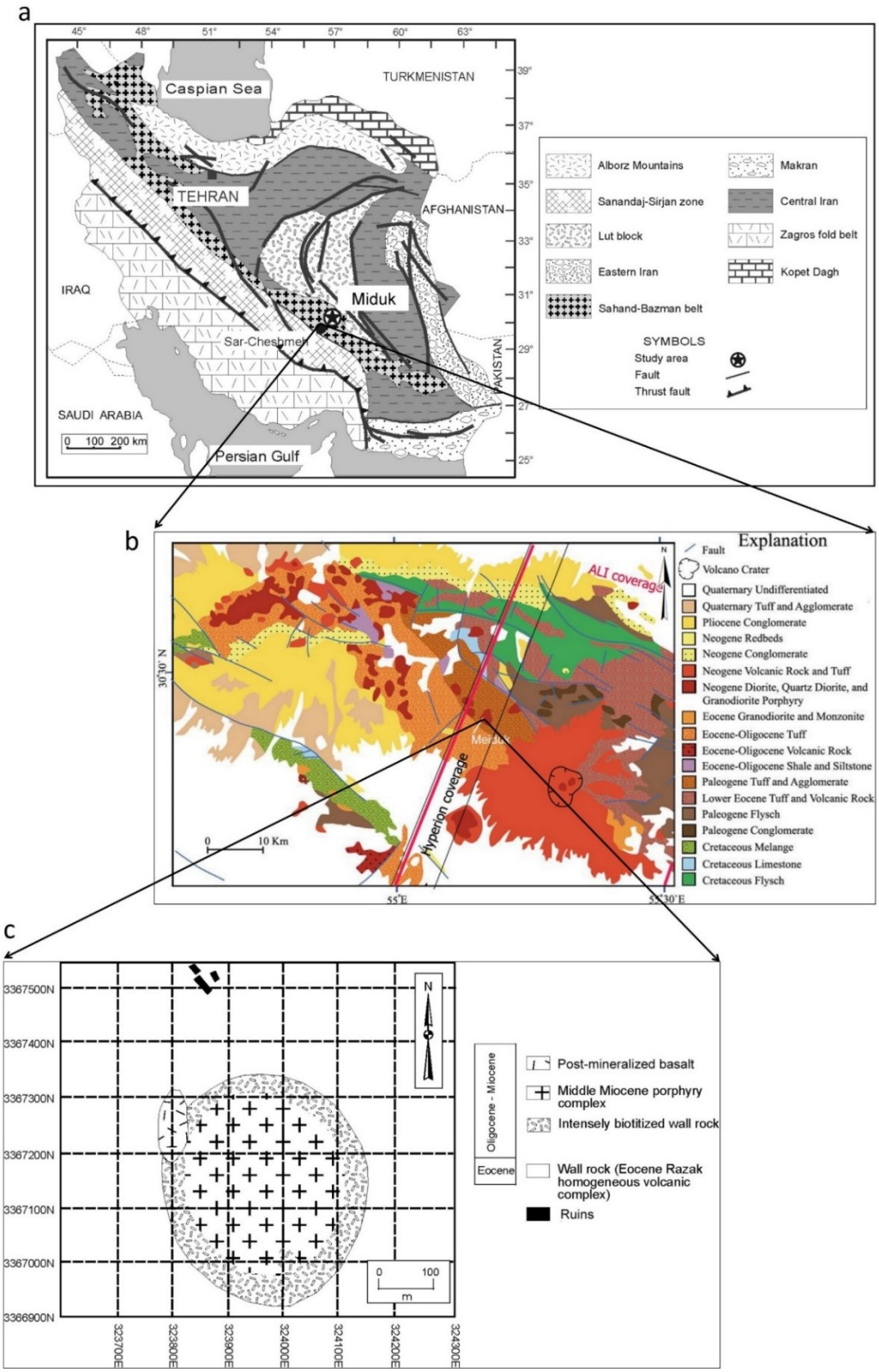

Figure 1. (a) Geological map of Iran showing major lithotectonic units [20-22], (b) Geological map of Miduk region [23-25] and the Earth Observing-1 (EO-1) coverage data, and (c) Detailed geological map of Miduk area displaying the distribution of different igneous suites [20, 26].

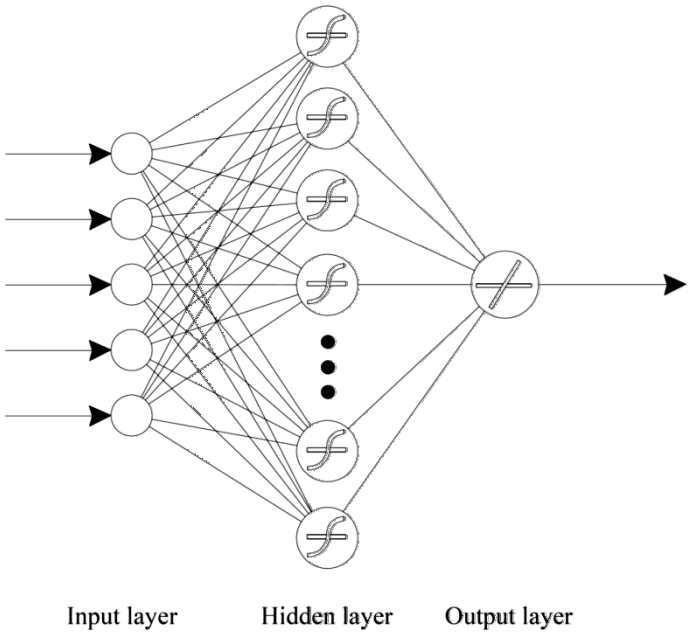

Figure 2. Architecture of ANNs with sigmoid activation function.

4.3. Concentration-volume (C-V) fractal model

The C-V fractal modeling, which was first proposed by Afzal et al. (2011) for identification of different mineralization zones in porphyry Cu deposits, can be generally expressed as [32]:

$$V(\rho \le \upsilon) \propto \rho^{-a1}; V(\rho \ge \upsilon) \propto \rho^{-a2} \quad (13)$$

where $V(\rho \le \upsilon)$ and $V(\rho \ge \upsilon)$ represent the volumes with concentration values (ρ) less than or equal to and greater than or equal to the contour values (υ); and a1 and a2 are the characteristic exponents. The contour value (υ) in this model explains the boundaries that separate various mineralized (alteration) zones and concentration populations. In this work, the OK and ANN outputs (block model) were processed by the C-V fractal method, and $V(\rho \le \upsilon)$ and $V(\rho \ge \upsilon)$ (the volumes enclosed by a concentration contour) were calculated in a 3D space [32].

5. Results and discussion

5.1. Statistical parameters and spatial variability analysis

Histogram and descriptive statistics of copper grades from 21,710 borehole samples in the hypogene zone of the Miduk PCD are displayed in Figure 3. The copper grade (Cu%) as a regionalized variable has no trend in any direction; it means that the Cu grade does not have any correlation with sample coordinates, so it fulfills the first-order stationary assumption (Figure 4). The Gaussian kriging method was not used in this work. Consequently, the data was not normalized and the raw data was utilized. The statistical, geostatistical, and visualization operations were conducted using the Microsoft Excel spreadsheet software and Datamine studios. Experimental semi-variograms of Cu grade, as an important tool for anisotropy investigation, were calculated for different directions with 10° vertical angular increments, 5° vertical angular tolerance, 30° horizontal angular increments, and 15° horizontal angular tolerance. The main directions resulting from variography are depicted in Figure 5. The results obtained show a mild anisotropy in the azimuth of 155 (major axis). The formulas of spherical models fitted to the main directions are as follow:

$$\gamma(h) = \begin{cases} 0 & h = 0 \\ C_0 + C\left(\frac{3}{2}\left(\frac{h}{a}\right) - \frac{1}{2}\left(\frac{h}{a}\right)^3\right) & 0 < h \le a \\ C_0 + C_1 & h > a \end{cases} \quad (14)$$

$$\gamma(h) = \begin{cases} 0 & h = 0 \\ 0.024 + 0.221\left(\frac{3}{2}\left(\frac{h}{300}\right) - \frac{1}{2}\left(\frac{h}{300}\right)^3\right) & 0 < h \le 300 \\ 0.245 & h > 300 \end{cases} \quad (15)$$

$$\gamma(h) = \begin{cases} 0 & h = 0 \\ 0.024 + 0.221\left(\frac{3}{2}\left(\frac{h}{342}\right) - \frac{1}{2}\left(\frac{h}{342}\right)^3\right) & 0 < h \le 342 \\ 0.245 & h > 342 \end{cases} \quad (16)$$

$$\gamma(h)=\begin{cases}0 & h=0\\ 0.024+0.221\left(\frac{3}{2}\left(\frac{h}{311}\right)-\frac{1}{2}\left(\frac{h}{311}\right)^{3}\right) & ,\ 0<h\le 311\\ 0.245 & h>311\end{cases} \quad (17)$$

where C_0 is the nugget constant, $C+C_0$ is the Sill, and a is the variogram range.

The omnidirectional semi-variogram of the copper grade data follows a spherical model, which reaches a sill of 0.213 $(\%)^2$ at a range of 389 m with a nugget effect of 0.031 $(\%)^2$, as shown in Figure 5-a. Three main directions of the search ellipsoid were chosen from experimental directional semi-variograms of Cu to create the best variography model for the ordinary kriging estimation (Figure 5-b). In order to evaluate the accuracy of the variogram model, in a process called the cross-validation, each one of the grade values was estimated using the data from the neighborhood. The scatter diagram between the actual and the estimated grades are represented in Figure 6.

5.2. Ok estimation

According to variography and the determined evaluation parameters, the OK model was generated on a 15 × 15 × 15 (m^3) grid in the hypogene zone of the Miduk PCD. There are many advantages in 3D modeling of grade in an ore deposit so that it leads to more reliable evaluations and judgments about different parts of the deposit. The horizontal plans of an OK model consisting of levels 1600, 1900, 2200, and 2500 m are displayed in Figure 7.

5.3. ANN estimation

5.3.1. Data processing

The available data was classified into two categories: (I) inputs (x,y,z) and (II) output (Cu grade). Afterwards, the dataset was divided into three sections including training (70%), validation (15%), and testing (15%). The validation dataset used in this work prevents the process from over-fitting and works like a criteria for early stopping the training process as the network performance (for training) reduce. The available data was randomly selected to breakdown into the determined datasets. Moreover, the available data was scaled into [0 1] because it should be in a suitable shape for NN training. Data processing and neural network modeling were conducted using MATLAB (R2014a).

5.3.2. MLP neural network

Trial-and-error is the most common way for assessment of the optimal structure of MLP. In this case, in order to find the optimal structure of NN, the network parameters such as the number of neurons in the hidden layer were changed, and by substitution of the inputs, the final NN structure was obtained. In other words, because there is no tool to find the best values for NN parameters, the only way is to run the different networks for various conditions, and select the best created one. The results of this process are shown in Table 1. The process was carried out with Levenberg-Marquardt (LM) as the training algorithm and tansig as the output function of neural network. Using the sigmoidal output functions, the continuous graded response neurons can be defined [31] (Tahmasebi and Hezarkhani, 2011).

After dividing the data into three sections (training, validation, and testing), as mentioned in the "Data processing" section, the validation dataset was used to test the network during the training process in which the process would stop if the training error increases.

After training the network, the testing process was conducted with a completely independent data. After building the networks with different numbers of neurons, their MSE (Mean Square Error) and R values (correlation coefficient) were collected to find the optimal structure (optimal number of neurons). According to Table 1, 3-24-1 is the best network structure with the lowest MSE (0.0027) and the maximum R (0.85) values. MLP parameters such as the number of neurons in the hidden layer can lead the NN to be more time-consuming and more complex. Also the lack of data is another common problem whose acquisition needs spending too much time and money. As a result, this method can be utilized under different conditions to find the complex relationship among the datasets.

By utilizing the created ANN, Cu values were estimated for each block center on a 15 × 15 × 15 (m^3) grid. Horizontal plans of the OK model in different levels (1600, 1900, 2200, and 2500 m) are displayed in Figure 8.

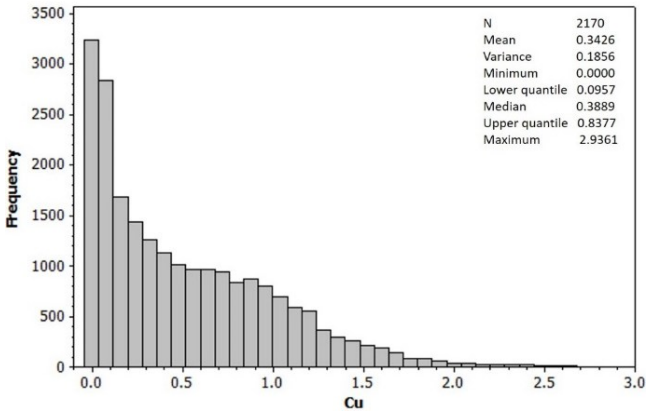

Figure 3. Histogram of the Cu data in hypogene zone of Miduk PCD.

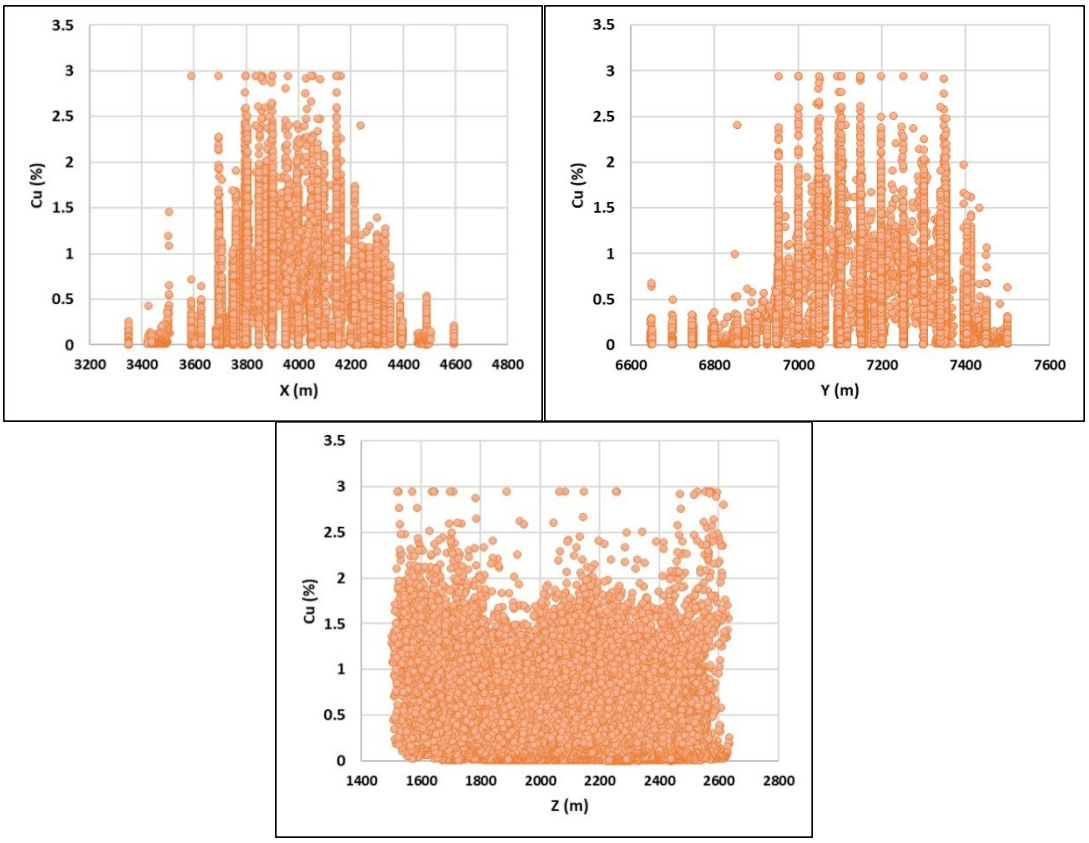

Figure 4. Variability of Cu concentration in (a) east-west, (b) north-south, and (c) depth directions within hypogene zone of Miduk PCD.

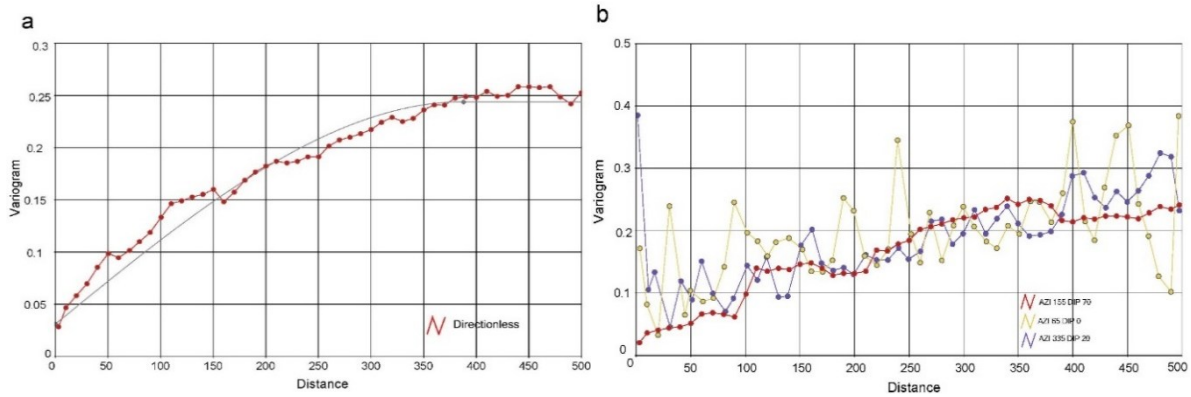

Figure 5. (a) Experimental semi-variogram (with appropriate fitted model) and (b) experimental directional semi-variograms (for 3 main directions of search ellipsoid) of the raw data in hypogene zone of Miduk PCD.

Table 1. Results of MLP for several neurons in hidden layer with their corresponding MSE and R values.

Number of neurons in hidden layer	MSE	R
4	0.0038	0.76
6	0.0037	0.78
8	0.0036	0.77
12	0.0031	0.83
16	0.0028	0.84
20	0.0031	0.84
24	0.0027	0.85
30	0.0029	0.85

Table 2. Cu threshold values identified using C-V fractal modeling for kriging and ANN results.

Estimation method	First (%)	Second (%)	Third (%)	Fourth (%)
kriging	0.479	1.023	1.514	1.905
ANN	0.871	2.089	3.548	4.467

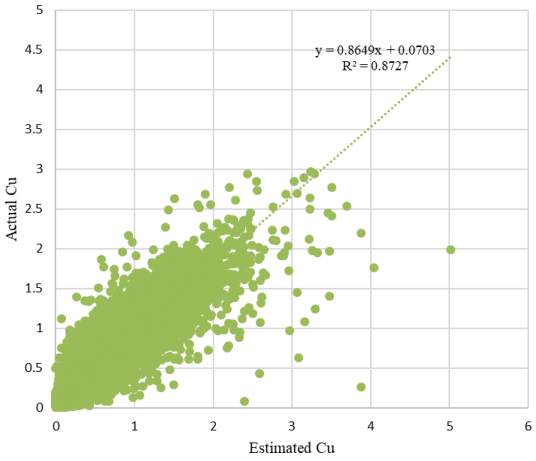

Figure 6. Cross-validation diagram to evaluate accuracy of variogram for kriging.

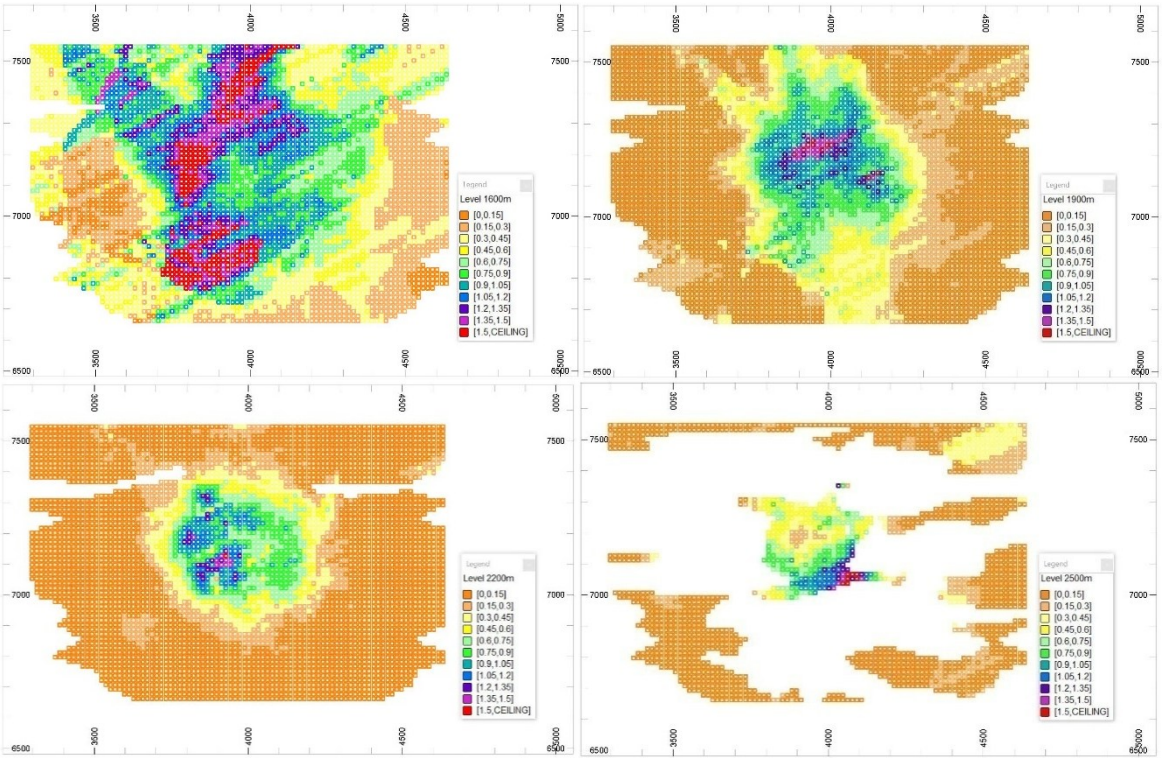

Figure 7. Horizontal plan of Cu concentration in different elevations (levels 1600, 1900, 2200, and 2500 m) resulting from kriging modeling within hypogene zone.

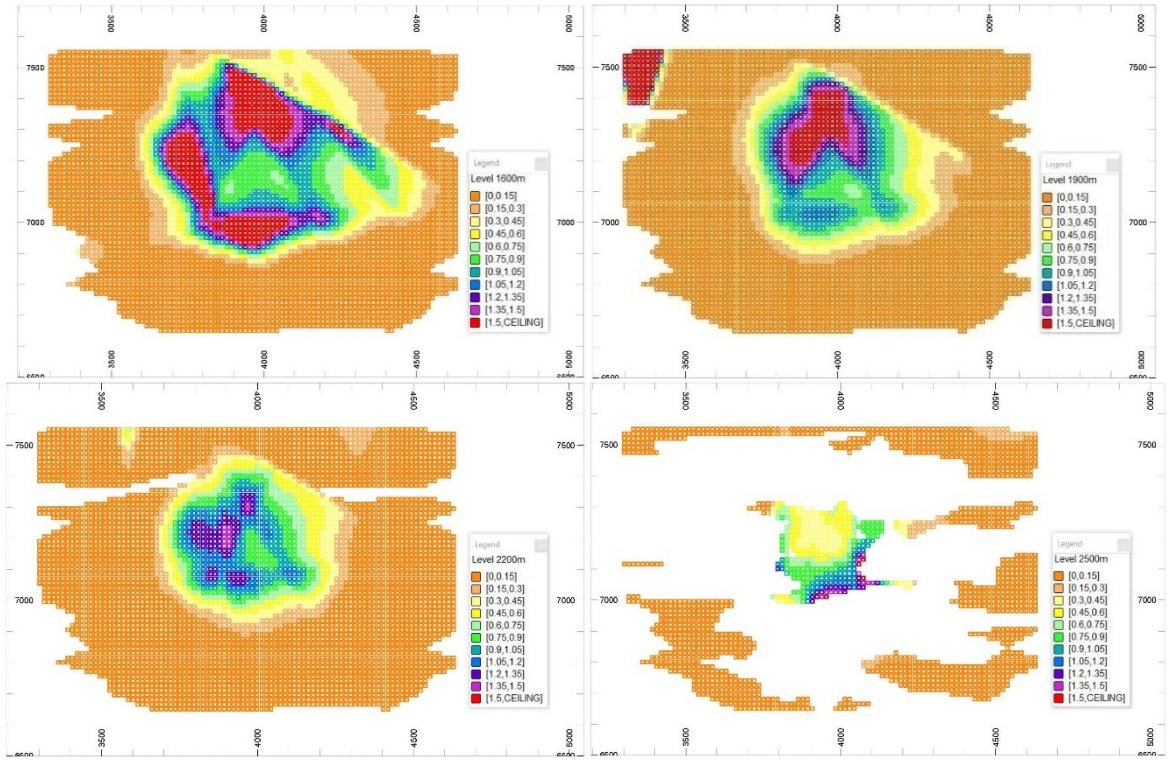

Figure 8. Horizontal plan of Cu concentration in different elevations (levels 1600, 1900, 2200, and 2500 m) resulting from ANN (with 24 neurons) modeling within hypogene zone.

5.4. Concentration-volume (C-V) fractal modeling

In order to find the relationship between Cu values and their corresponding volumes, the volumes were calculated based on the kriging and ANN results. The C-V log-log plots shown in Figure 9 depict a power-law relationship between the copper values and volumes. The log-log plot of ANN shows four threshold values equal to 0.871%, 2.089%, 3.548%, and 4.467%; additionally, four thresholds were identified in 0.479%, 1.023%, 1.514%, and 1.905% of Cu value for the kriging C-V plot, as provided in Figure 9 and Table 2.

According to the C-V modeling, the 3D model of hypogene zone was generated for the kriging and ANN outputs. The phyllic and propylitic alteration zones are weakly mineralized compared with the potassic zone in porphyry deposits [78, 101, 102]. Based on the C-V fractal modeling (3D model and vertical views) on the results of Kriging and ANN, Cu values less than 0.871% (ANN) and 0.479% (kriging) are the most likely periods for the phyllic alteration zone (Figures 10 and 11).

In the geological model proposed by Lowell and Guilbert (1970) for Cu porphyry deposits, the potassic alteration zone, which occurs in the central part of the hypogene zone, hosts the high-grade Cu mineralization. According to the C-V fractal models, it seems that the Cu threshold values upper than 0.871% (especially the data between 0.871% and 2.089%) in ANN model and also the values upper than 0.479% (especially the data between 0.479% and 1.023%) in the kriging model can indicate the potassic alteration zone [78].

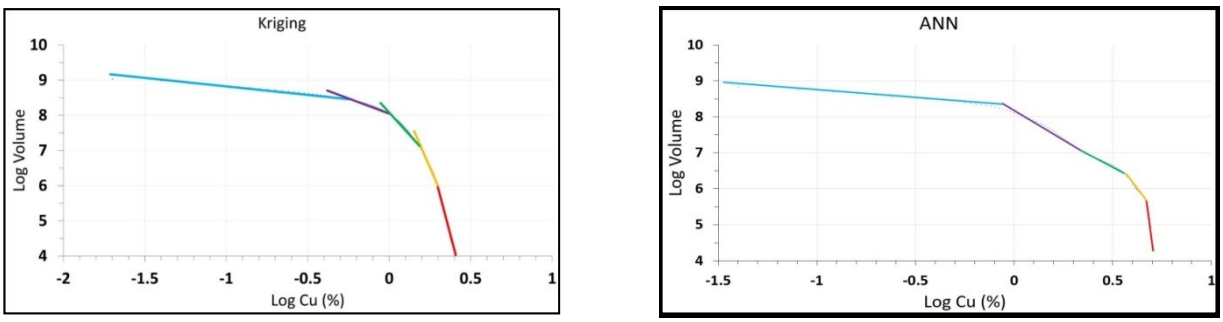

Figure 9. C-V fractal log-log plots resulting from kriging and ANN modelings within hypogene zone.

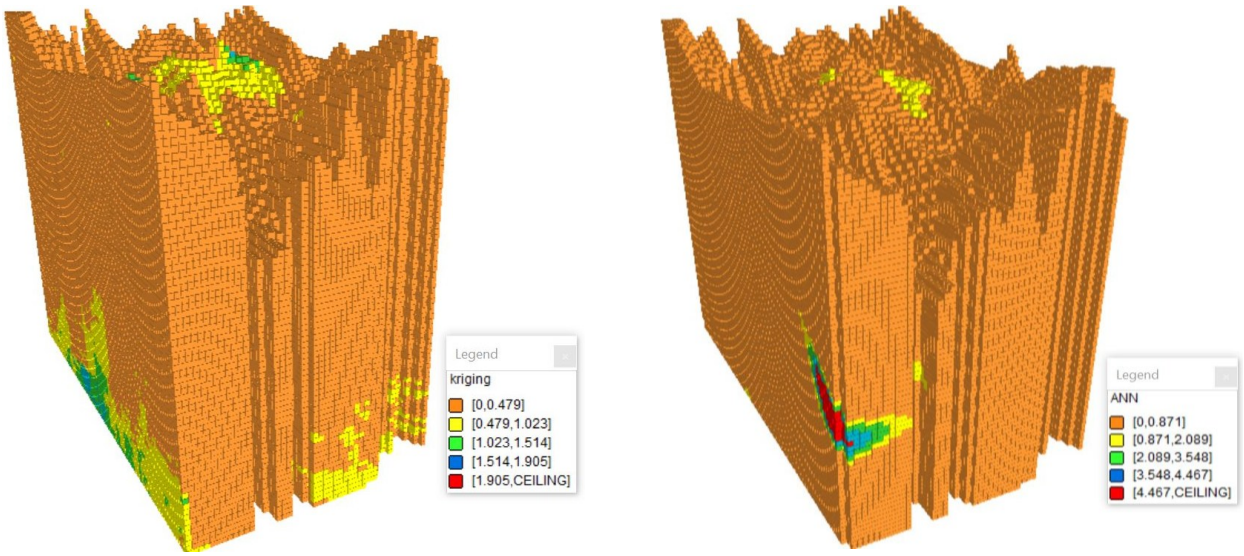

Figure 10. 3D view of kriging and ANN models in hypogene zone of Miduk PCD, considering the thresholds obtained from C-V fractal modeling.

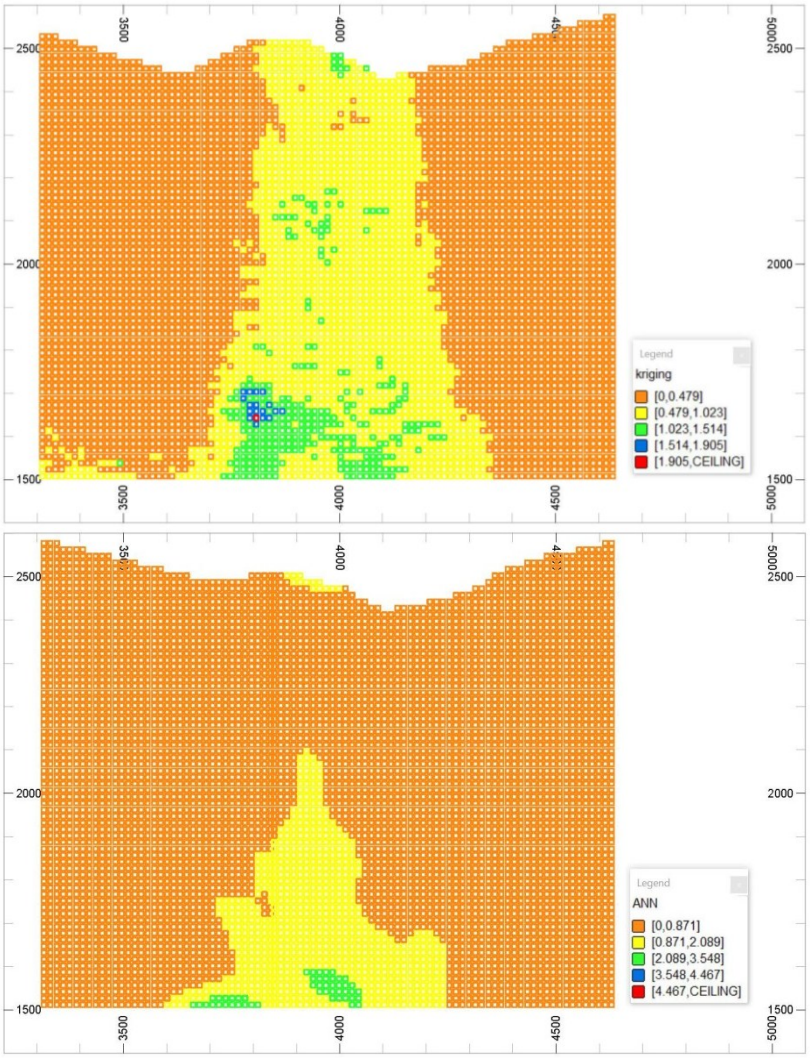

Figure 11. Vertical view of kriging and ANN models in hypogene zone of Miduk PCD considering the thresholds obtained from C-V fractal modeling.

5.5. Comparison of fractal and alteration model of deposit

In order to validate the results obtained through the C-V fractal modeling, the models were compared against the 3D alteration zone models of the hypogene zone of the Miduk PCD comprising the phyllic, propylitic, and potassic zones (Figure 12). The models were generated by applying the Datamine studios software and the geological drill core data.

An analytical method was proposed by Carranza (2011) to compare two binary models (in this case, C-V and alteration models) and to find the spatial correlations between them [103]. In this method, in order to find the common voxels between the C-V fractal results and each alteration zone, an intersection operation was carried out and the number of four classes of overlapping zones were found (Table 3). With respect to the geological data, Type 1 and Type 2 errors (T1E and T2E), and the overall accuracy (OA) were estimated for each alteration zone utilizing the numbers obtained in the previous step.

Comparing the phyllic alteration zone in the geological model and the range of values distinguished by the thresholds in C-V modeling showed that Cu values less than 0.479% (kriging) and 0.871% (ANN) were more correlated with the alteration zone. The comparison revealed that the phyllic zone had more overlapped voxels with the values less than 0.479% (kriging) compared with the other results because the OA value of this threshold (0.829) was higher than the others, as presented in Tables 3 and 4. The validation matrix of propylitic alteration for fractal modeling of kriging and ANN revealed that OA varied between 0.151 and 0.988 but none of the highest OAs had a low T1E. In this case, the high value of OA with a low T1E is caused by the lack of data on the propylitic alteration of hypogene zone, by which none of the thresholds can properly distinguish the propylitic zone (Tables 5 and 6).

According to the intersection operation between the potassic zone in the 3D geological model and the C-V fractal model of kriging and NN, the best correlation with the maximum amount of OA (0.779) occurred in an interval between 0.479% and 1.023% of Cu (kriging), as presented in Tables 7 and 8. As a result, the model obtained by kriging is appropriate for the separation of phyllic and potassic alterations but due to the lack of propylitic alteration in the hypogene zone of the Miduk mine, the models could not properly distinguish the alteration zone.

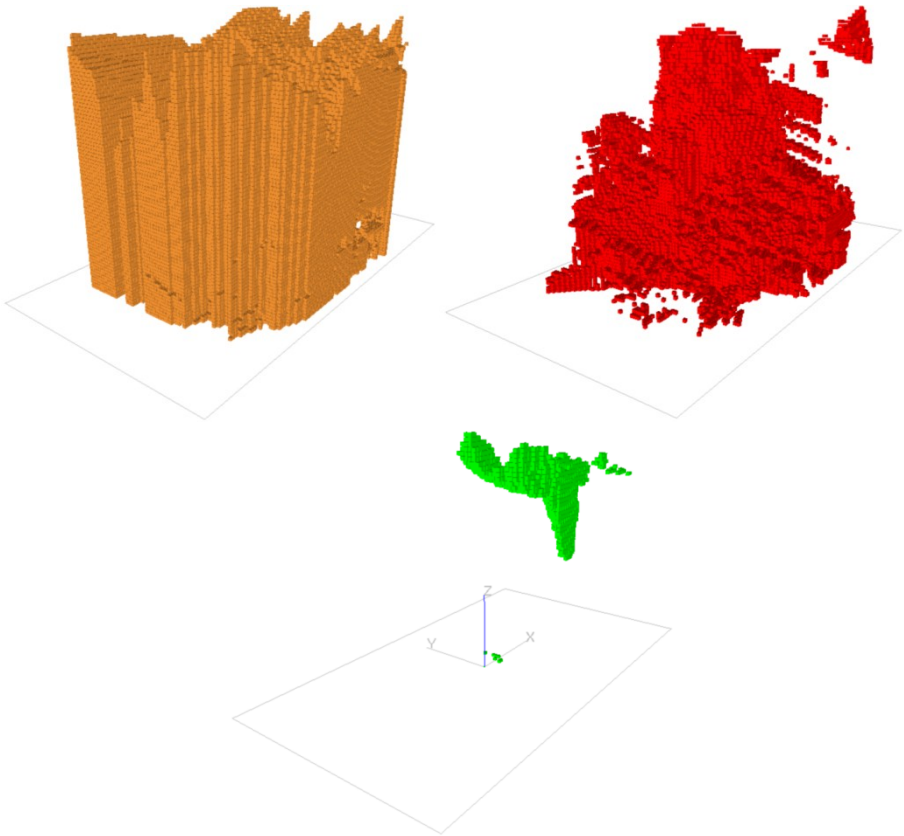

Figure 12. Alteration zones in hypogene zone of Miduk PCD based on the geological model: (orange) phyllic, (red) potassic, and (Green) propylitic.

Table 3. Matrix for calculating the spatial correlation between the alteration model derived from the C-V fractal modeling of ANN results and the geological model. A and D show the numbers of voxels that are estimated correctly. On the other hand, B and C represent the number of voxels with different results in the C-V fractal compared with the geological model [103] (Carranza, 2011). Overall accuracy (OA), Type I and Type II errors (T1E and T2E, respectively), resulted from the comparison between the phyllic alteration zone in the 3D geological model, and the first Cu threshold values in the C–V fractal model of ANN results in the hypogene zone.

Fractal model	Inside zone / Outside zone	Geological model			
		Inside zone		Outside zone	
		True positive (A)		False positive (B)	
		False negative (C)		True negative (D)	
		Type I Error = C/(A +C)		Type II Error = B/(B + D)	
		Overall accuracy = (A + D)/(A + B + C + D)			
		Phyllic alteration of geological model			
		Inside zones		Outside zones	
Cu ≤ 0.871	Inside zones	A	219607	B	83900
	Outside zones	C	7083	D	42111
		T1E	0.03	T2E	0.66
		OA	0.74		
0.871 <Cu ≤2.089	Inside zones	A	5477	B	40305
	Outside zones	C	221213	D	85706
		T1E	0.97	T2E	0.32
		OA	0.26		
2.089 < Cu ≤ 3.548	Inside zones	A	1350	B	1509
	Outside zones	C	225340	D	124502
		T1E	0.99	T2E	0.01
		OA	0.36		
3.548 < Cu ≤ 4.467	Inside zones	A	246	B	297
	Outside zones	C	226444	D	125714
		T1E	0.99	T2E	0.002
		OA	0.36		
Cu > 4.467	Inside zones	A	10	B	0
	Outside zones	C	226680	D	126011
		T1E	0.99	T2E	0
		OA	0.36		

Table 4. OA, T1E, and T2E resulting from the comparison between the Phyllic alteration zone in the 3D geological model and the threshold values of Cu in the C–V fractal model of realizations and kriging results in the hypogene zone.

		Phyllic alteration of geological model			
		Inside zones		Outside zones	
Cu ≤ 0.479	Inside zones	A	211751	B	45215
	Outside zones	C	14939	D	80796
		T1E	0.06	T2E	0.36
		OA	0.83		
0.479 < Cu ≤ 1.023	Inside zones	A	11942	B	53575
	Outside zones	C	214748	D	72436
		T1E	0.95	T2E	0.42
		OA	0.24		
1.023 < Cu ≤ 1.514	Inside zones	A	1947	B	24017
	Outside zones	C	224743	D	101994
		T1E	0.99	T2E	0.19
		OA	0.29		
1.514 < Cu ≤ 1.905	Inside zones	A	894	B	2817
	Outside zones	C	225796	D	123194
		T1E	0.99	T2E	0.02
		OA	0.35		
Cu > 1.905	Inside zones	A	156	B	387
	Outside zones	C	226534	D	125624
		T1E	0.99	T2E	0
		OA	0.36		

Table 5. OA, T1E, and T2E resulting from comparing the propylitic alteration zone in the 3D geological model and the threshold values of Cu in the C–V fractal model of realizations and ANN results in hypogene zone.

		Propylitic alteration of geological model			
		Inside zones		Outside zones	
Cu ≤ 0.871	Inside zones	A	4158	B	299349
	Outside zones	C	1	D	49193
		T1E	0.000	T2E	0.86
		OA	0.15		
0.871 < Cu ≤ 2.089	Inside zones	A	1	B	45781
	Outside zones	C	4158	D	302761
		T1E	0.99	T2E	0.13
		OA	0.86		
2.089 < Cu ≤ 3.548	Inside zones	A	0	B	2859
	Outside zones	C	4159	D	345683
		T1E	1	T2E	0.01
		OA	0.98		
3.548 < Cu ≤ 4.467	Inside zones	A	0	B	543
	Outside zones	C	4159	D	347999
		T1E	1	T2E	0.001
		OA	0.99		
Cu > 4.467	Inside zones	A	0	B	10
	Outside zones	C	4159	D	348532
		T1E	1	T2E	0.000
		OA	0.99		

Table 6. OA, T1E, and T2E resulting from comparing the propylitic alteration zone in the 3D geological model and the threshold values of Cu in the C–V fractal model of realizations and kriging results in hypogene zone.

		Propylitic alteration of geological model			
		Inside zones		Outside zones	
Cu ≤ 0.479	Inside zones	A	4153	B	252813
	Outside zones	C	6	D	95729
		T1E	0.001	T2E	0.72
		OA	0.28		
0.479 < Cu ≤ 1.023	Inside zones	A	6	B	65511
	Outside zones	C	4153	D	283031
		T1E	1	T2E	0.19
		OA	0.80		
1.023 < Cu ≤ 1.514	Inside zones	A	0	B	25964
	Outside zones	C	4159	D	322578
		T1E	1	T2E	0.07
		OA	0.91		
1.514 < Cu ≤ 1.905	Inside zones	A	0	B	3711
	Outside zones	C	4159	D	344831
		T1E	1	T2E	0.01
		OA	0.98		
Cu > 1.905	Inside zones	A	0	B	543
	Outside zones	C	4159	D	347999
		T1E	1	T2E	0.001
		OA	0.99		

Table 7. OA, T1E, and T2E resulting from the comparison between the Potassic alteration zone in the 3D geological model and the threshold values of Cu in the C–V fractal model of realizations and ANN results in hypogene zone.

		Potassic alteration of geological model			
		Inside zones		Outside zones	
Cu ≤ 0.871	Inside zones	A	72802	B	230705
	Outside zones	C	39074	D	10120
		T1E	0.35	T2E	0.96
		OA	0.23		
0.871 <Cu ≤2.089	Inside zones	A	37953	B	7829
	Outside zones	C	73923	D	232996
		T1E	0.66	T2E	0.03
		OA	0.77		
2.089 < Cu ≤ 3.548	Inside zones	A	1092	B	1767
	Outside zones	C	110784	D	239058
		T1E	0.99	T2E	0.01
		OA	0.68		
3.548 < Cu ≤ 4.467	Inside zones	A	29	B	514
	Outside zones	C	111847	D	240311
		T1E	0.99	T2E	0.002
		OA	0.68		
Cu > 4.467	Inside zones	A	0	B	10
	Outside zones	C	111876	D	240815
		T1E	1	T2E	0.000
		OA	0.68		

Table 8. OA, T1E, and T2E resulting from the comparison between the Potassic alteration zone in the 3D geological model and the threshold values of Cu in the C–V fractal model of realizations and kriging results in hypogene zone.

		Potassic alteration of geological model			
		Inside zones		Outside zones	
Cu ≤ 0.479	Inside zones	A	36675	B	220291
	Outside zones	C	75201	D	20534
		T1E	0.67	T2E	0.91
		OA	0.16		
0.479 < Cu ≤ 1.023	Inside zones	A	49807	B	15710
	Outside zones	C	62069	D	225115
		T1E	0.55	T2E	0.06
		OA	0.78		
1.023 < Cu ≤1.514	Inside zones	A	22743	B	3221
	Outside zones	C	89133	D	237604
		T1E	0.8	T2E	0.01
		OA	0.74		
1.514 < Cu ≤ 1.905	Inside zones	A	2409	B	1302
	Outside zones	C	109467	D	239523
		T1E	0.98	T2E	0.002
		OA	0.68		
Cu > 1.905	Inside zones	A	242	B	301
	Outside zones	C	111634	D	240524
		T1E	1	T2E	0.001
		OA	0.68		

6. Conclusions

In order to determine the spatial structures of ore zones, the geological models should be constructed based on the borehole data. Ore grades are not usually considered in the modeling methods, while variations in this parameter are the most obvious and salient features. Uncertainty occurs in logging a drill core, alteration recognition during the geological study, and in the correlation detected between the grade distribution and the alteration patterns in hydrothermal models. This reveals that ore grades can be used to find the spatial structure of the alteration zones. The quantitative models produced in this process, resulted in a qualitative model of alterations. In order to construct this model, multiple mathematical analyses such as the kriging estimation and data processing tools like artificial neural network can be used.

Ordinary kriging, as an appropriate geostatistical estimator and the most useful technique among the different kriging methods, and artificial neural network, as a powerful data mining tool, can be good choices for mathematical modeling.

In this work, the ordinary kriging, artificial neural networks, and C-V fractal models were applied to delineate different alteration zones in the hypogene zone of the Miduk porphyry copper deposit, SE Iran. Applying the C-V fractal technique on the grade models derived from the estimations led to the separation of grade populations, and consequently, detecting different alteration zones. Between the methods, although ANN is faster and requires less expert knowledge, kriging shows the best result for delineating phyllic (OA = 0.83) and potassic (OA = 0.78) alteration zones. According to the overall accuracy resulting in the validation process of C-V fractal thresholds, the performance of kriging and neural network in delineation of the propylitic alteration zone was almost the same. Moreover, due to the lack of data, none of these results including the C-V fractal modeling on kriging and neural network outputs was suitable for delineating the propylitic alteration zone.

The correlation between the results and the 3D model of alteration zones in the hypogene zone reveals that the phyllic and potassic alterations are highly correlated with Cu values of less than 0.479% and the values between 0.479% and 1.023%, respectively. Furthermore, there was no proper relation between the propylitic alteration and the Cu values. As it was expected, the obtained models supported the Lowell-Guilbert (1970) model of alteration zones in porphyry copper deposits [78].

Acknowledgments

The authors appreciate the National Iranian Copper Industries Company (NICICO) for funding the project and express their gratitude to Mrs. Zahra Abbasloo and Mr. Mojtaba Dehghani Javazm from the Miduk mine for their effective support. The authors also would like to thank Mr. Bashir Shokouh Saljooghi and Mr. Mohammad Amin Shabani for their useful helps.

Funding

This work was supported by the National Iranian Copper Industries Company.

References

[1]. Tutmez, B. (2007). An uncertainty oriented fuzzy methodology for grade estimation. Computers & Geosciences. 33 (2): 280-288.

[2]. Kapageridis, I.K. and Denby, B. (1998). Neural network modelling of ore grade spatial variability. In ICANN 98 (pp. 209-214). Springer, London.

[3]. Li, X.L., Xie, Y.L., Guo, Q.J. and Li, L.H. (2010). Adaptive ore grade estimation method for the mineral deposit evaluation. Mathematical and Computer Modelling. 52 (11-12): 1947-1956.

[4]. Journel, A.G. and Huijbregts, C.J. (1978). Mining geostatistics. Academic press.

[5]. Rendu, J.M. (1979). Kriging, logarithmic Kriging and conditional expectation: comparison of theory with actual results. Proc., 16th APCOM Symposium. Tucson, Arizona. pp. 199-212.

[6]. Chowdhury, M., Alouani, A. and Hossain, F. (2010). Comparison of ordinary kriging and artificial neural network for spatial mapping of arsenic contamination of groundwater. Stochastic Environmental Research and Risk Assessment. 24 (1): 1-7.

[7]. Hengl, T. (2009). A practical guide to geostatistical mapping. Vol. 52. 15 P.

[8]. Mpanza, M. (2015). A comparison of ordinary and simple kriging on a PGE resource in the Eastern limb of the Bushveld complex (Doctoral dissertation). 19 P.

[9]. Armstrong, M. (1998). Basic linear geostatistics. Springer Science & Business Media.

[10]. Emery, X. (2005). Simple and ordinary multigaussian kriging for estimating recoverable reserves. Mathematical Geology. 37 (3): 295-319.

[11]. Daya, A.A. (2015). Ordinary kriging for the estimation of vein type copper deposit: A case study of the Chelkureh, Iran. Journal of Mining and Metallurgy A: Mining. 51 (1): 1-14.

[12]. Chilès, J.P. and Delfiner, P. (2012). Geostatistics: Modeling Spatial Uncertainty. Wiley New York.

[13]. Khakestar, M.S., Madani, H., Hassani, H. and Moarefvand, P. (2013). Determining the best search neighbourhood in reserve estimation, using geostatistical method: A case study anomaly No 12A iron deposit in central Iran. Journal of the Geological Society of India. 81 (4): 581-585.

[14]. Strebelle, S. (2002). Conditional simulation of complex geological structures using multiple-point statistics. Mathematical geology. 34 (1): 1-21.

[15]. Reis, A., Sousa, A. and Fonseca, E.C. (2003). Application of geostatistical methods in gold geochemical anomalies identification (Montemor-O-Novo, Portugal). Journal of Geochemical Exploration. 77: 45-63.

[16]. Pyrcz, M.J. and Deutsch, C.V. (2014). Geostatistical reservoir modeling. Oxford university press.

[17]. Paravarzar, S., Emery, X. and Madani, N. (2015). Comparing sequential Gaussian and turning bands algorithms for cosimulating grades in multi-element deposits. Comptes Rendus Geoscience. 347 (2): 84-93.

[18]. Shahbeik, S., Afzal, P., Moarefvand, P. and Qumarsy, M. (2014). Comparison between Ordinary Kriging (OK) and inverse distance weighted (IDW) based on estimation error. Case study: Dardevey iron ore deposit, NE Iran. Arabian Journal of Geosciences. 7 (9): 3693-3704.

[19]. Tahmasebi, P. and Hezarkhani, A. (2012). A hybrid neural networks-fuzzy logic-genetic algorithm for grade estimation. Computers & geosciences. 42: 18-27.

[20]. Hezarkhani, A. (2008). Hydrothermal evolution of the Miduk porphyry copper system, Kerman, Iran: a fluid inclusion investigation. International Geology Review. 50 (7): 665-684.

[21]. Stöcklin, J. and Setudenia, A. (1972). Lexique Stratigraphique International, Volume III. Paris, France, ASIE Centre National De La Recherche Scientifique. 75 P.

[22]. Stöcklin, J. (1977). Structural correlation of the Alpine ranges between Iran and Central Asia: Memoire Hors-Serie. de la Société Géologique de France. 8: 333-353.

[23]. Beiranvand Pour, A., and Hashim, M. (2011). The Earth Observing-1 (EO-1) satellite data for geological mapping, southeastern segment of the Central Iranian Volcanic Belt, Iran. International Journal of the Physical Sciences. 6 (33): 7638-7650.

[24]. Hubner, H. (1969). Geological map of Iran sheet no. 6, southeast Iran: Tehran, National Iranian Oil Company, scale 1:1,000,000.

[25]. Mars, J.C. and Rowan, L.C. (2006). Regional mapping of phyllic- and argillic-altered rocks in the Zagros magmatic arc, Iran using Advanced Spaceborne Thermal Emission and Reflection Radiometer (ASTER) data and logical operator algorithms. Geosphere. 2 (3): 161-186.

[26]. Hassanzadeh, J. (1993). Metallogenic and tectono-magmatic events in the SE sector of the Cenozoic active continental margin of Iran (Shahr e Babak area, Kerman province). Unpublished Ph. D. thesis, University of California, Los Angeles.

[27]. Andries, A. (2007). Computational Intelligence, seconded. University of Pretoria, South Africa.

[28]. Baykan, N.A. and Yılmaz, N. (2010). Mineral identification using color spaces and artificial neural networks. Computers & Geosciences. 36 (1): 91-97.

[29]. Shokooh Saljooghi, B. and Hezarkhani, A. (2014). Comparison of WAVENET and ANN for predicting the porosity obtained from well log data. Journal of Petroleum Science and Engineering. 123: 172-182.

[30]. Zaremotlagh, S. and Hezarkhani, A. (2017). The use of decision tree induction and artificial neural networks for recognizing the geochemical distribution patterns of LREE in the Choghart deposit, Central Iran. Journal of African Earth Sciences. 128: 37-46.

[31]. Tahmasebi, P. and Hezarkhani, A. (2011). Application of a Modular Feedforward Neural Network for Grade Estimation. Natural Resources Research. 20: 25-32.

[32]. Afzal, P., Alghalandis, Y.F., Khakzad, A., Moarefvand, P. and Omran, N.R. (2011). Delineation of mineralization zones in porphyry Cu deposits by fractal concentration–volume modeling. Journal of Geochemical Exploration. 108 (3): 220-232.

[33]. Yasrebi, A.B., Afzal, P., Wetherelt, A., Foster, P. and Esfahanipour, R. (2013). Correlation between geology and concentration-volume fractal models: significance for Cu and Mo mineralized zones separation in the Kahang porphyry deposit (Central Iran). Geologica Carpathica. 64 (2): 153-163.

[34]. Davis, J.C. (2002). Statistics and data analysis in Geology, 3rd ed. John Wiley & Sons Inc., New York.

[35]. Mandelbrot, B.B. (1983). The Fractal Geometry of Nature (Updated and Augmented Edition). W.H. Freeman, San Francisco.

[36]. Afzal, P., Khakzad, A., Moarefvand, P., Omran, N.R., Esfandiari, B. and Alghalandis, Y.F. (2010). Geochemical anomaly separation by multifractal modeling in Kahang (Gor Gor) porphyry system, Central Iran. Journal of Geochemical Exploration. 104 (1): 34-46.

[37]. Agterberg, F.P. (1995). Multifractal modeling of the sizes and grades of giant and supergiant deposits. Int. Geol. Rev. 37: 1-8.

[38]. Cheng, Q., Agterberg, F.P. and Ballantyne, S.B. (1994). The separation of geochemical anomalies from background by fractal methods. J. Geochem. Explor. 51: 109-130.

[39]. Deng, J., Wang, Q., Yang, L., Wang, Y., Gong, Q. and Liu, H. (2010). Delineation and explanation of geochemical anomalies using fractal models in the Heqing area, Yunnan Province, China. Journal of Geochemical Exploration. 105 (3): 95-105.

[40]. Goncalves, M.A., Mateus, A. and Oliveira, V. (2001). Geochemical anomaly separation by multifractal modelling. Journal of Geochemical Exploration. 72 (2): 91-114.

[41]. Hassanpour, S. and Afzal, P. (2013). Application of concentration–number (C–N) multifractal modeling for geochemical anomaly separation in Haftcheshmeh porphyry system, NW Iran. Arabian Journal of Geosciences. 6 (3): 957-970.

[42]. Li, C., Ma, T. and Shi, J. (2003). Application of a fractal method relating concentrations and distances for separation of geochemical anomalies from background. J. Geochem. Explor. 77: 167-175.

[43]. Rahmati, A., Afzal, P., Abrishamifar, S.A. and Sadeghi, B. (2015). Application of concentration–number and concentration–volume fractal models to delineate mineralized zones in the Sheytoor iron deposit, Central Iran. Arabian Journal of Geosciences. 8 (5): 2953-2965.

[44]. Shen, W. and Zhao, P. (2002). Theoretical study of statistical fractal model with applications to mineral resource prediction. Computers & Geosciences. 28 (3): 369-376.

[45]. Yuan, F., Li, X., Jowitt, S.M., Zhang, M., Jia, C., Bai, X. and Zhou, T. (2012). Anomaly identification in soil geochemistry using multifractal interpolation: A case study using the distribution of Cu and Au in soils from the Tongling mining district, Yangtze metallogenic belt, Anhui province, China. Journal of Geochemical Exploration. 116: 28-39.

[46]. Zuo, R., Cheng, Q. and Xia, Q. (2009). Application of fractal models to characterization of vertical distribution of geochemical element concentration. J. Geochem. Explor. 102: 37-43.

[47]. Afzal, P., Ahari, H.D., Omran, N.R. and Aliyari, F. (2013). Delineation of gold mineralized zones using concentration–volume fractal model in Qolqoleh gold deposit, NW Iran. Ore Geology Reviews. 55: 125-133.

[48]. Afzal, P., Ghasempour, R., Mokhtari, A.R. and Haroni, H.A. (2015). Application of Concentration-Number and Concentration-Volume Fractal Models to Recognize Mineralized Zones in North Anomaly Iron Ore Deposit, Central Iran. Archives of Mining Sciences. 60 (3): 777-789.

[49]. Afzal, P., Mirzaei, M., Yousefi, M., Adib, A., Khalajmasoumi, M., Zarifi, A.Z., Foster, P. and Yasrebi, A.B. (2016). Delineation of geochemical anomalies based on stream sediment data utilizing fractal modeling and staged factor analysis. Journal of African Earth Sciences. 119: 139-149.

[50]. Afzal, P., Tehrani, M.E., Ghaderi, M. and Hosseini, M.R. (2016). Delineation of supergene enrichment, hypogene and oxidation zones utilizing staged factor analysis and fractal modeling in Takht-e-Gonbad porphyry deposit, SE Iran. Journal of Geochemical Exploration. 161: 119-127.

[51]. Dahooei, A.H., Afzal, P., Lotfi, M. and Jafarirad, A. (2016). Identification of mineralized zones in the Zardu area, Kushk SEDEX deposit (Central Iran), based on geological and multifractal modeling. Open Geosciences. 8 (1): 143-153.

[52]. Parsa, M., Maghsoudi, A., Yousefi, M. and Carranza, E.J.M. (2017). Multifractal interpolation and spectrum–area fractal modeling of stream sediment geochemical data: Implications for mapping exploration targets. Journal of African Earth Sciences. 128: 5-15.

[53]. Parsa, M., Maghsoudi, A., Yousefi, M. and Sadeghi, M. (2017). Multifractal analysis of stream sediment geochemical data: Implications for hydrothermal nickel prospection in an arid terrain, eastern Iran. Journal of Geochemical Exploration. 181: 305-317.

[54]. Rajoli, M.E., Afzal, P. and Moarefvand, P. (2015). Classification of mineralized veins using concentration volume (C–V) fractal modeling: a case study from Chah-Mesi Cu–Au vein deposit, SE Iran. Arabian Journal of Geosciences. 8 (10): 8249-8262.

[55]. Sim, B.L., Agterberg, F.P. and Beaudry, C. (1999). Determining the cutoff between background and relative base metal smelter contamination levels using multifractal methods. Computers & Geosciences. 25 (9): 1023-1041.

[56]. Cheng, Q. (1995). The perimeter-area fractal model and its application to geology. Mathematical Geology. 27 (1): 69-82.

[57]. Cheng, Q., Xu, Y. and Grunsky, E. (1999). Integrated spatial and spectral analysis for geochemical anomaly separation. Proc., Conference of the International Association for Mathematical Geology, S.J. Lippard, A. Naess, R. Sinding-Larsen (Eds.) Trondheim, Norway. 1: 87-92.

[58]. Afzal, P., Alghalandis, Y.F., Moarefvand, P., Omran, N.R. and Haroni, H.A. (2012). Application of power-spectrum–volume fractal method for detecting hypogene, supergene enrichment, leached and barren

zones in Kahang Cu porphyry deposit, Central Iran. Journal of Geochemical Exploration. 112: 131-138.

[59]. Sadeghi, B., Madani, N. and Carranza, E.J.M. (2015). Combination of geostatistical simulation and fractal modeling for mineral resource classification. Journal of Geochemical Exploration. 149: 59-73.

[60]. Sillitoe, R.H. (2010). Porphyry copper systems. Economic geology. 105 (1): 3-41.

[61]. Barton, M.D., Staude, J.M., Zürcher, L. and Megaw, P.K. (1995). Porphyry copper and other intrusion-related mineralization in Mexico. Porphyry copper deposits of the American Cordillera: Arizona Geological Society Digest. 20: 487-524.

[62]. John, D.A., Ayuso, R.A., Barton, M.D., Blakely, R.J., Bodnar, R.J., Dilles, J.H., ... and Seal, R.R. (2010). Porphyry copper deposit model, chap. B of Mineral deposit models for resource assessment. US Geological Survey Scientific Investigations Report. 169 P.

[63]. Rusk, B.G., Reed, M.H. and Dilles, J.H. (2008). Fluid inclusion evidence for magmatic-hydrothermal fluid evolution in the porphyry copper-molybdenum deposit at Butte, Montana. Economic Geology. 103 (2): 307-334.

[64]. Sillitoe, R.H., Tolman, J. and Van Kerkvoort, G. (2013). Geology of the Caspiche porphyry gold-copper deposit, Maricunga Belt, Northern Chile. Economic Geology. 108 (4): 585-604.

[65]. Berberian, M. and King, G.C.P. (1981). Towards a paleogeography and tectonic evolution of Iran. Canadian Journal of Earth Sciences. 18 (2): 210-265.

[66]. Niazi, M., Asudeh, I., Ballard, G., Jackson, J., King, G. and McKenzie, D. (1978). The depth of seismicity in the Kermanshah region of the Zagros Mountains (Iran). Earth and Planetary Science Letters. 40 (2): 270-274.

[67]. Pourhosseini, F. (1983). Petrogenesis of Iranian plutons, a study of Natanz and Bazman intrusive complexes. Rep. Iran. Geol. survey.

[68]. Hezarkhani, A. (2006). Alteration/mineralization and controls of chalcopyrite dissolution/deposition in the Raigan porphyry system, Bam-Kerman, Iran. International Geology Review. 48 (6): 561-572.

[69]. Hezarkhani, A. (2006). Hydrothermal evolution of the Sar-Cheshmeh porphyry Cu–Mo deposit, Iran: evidence from fluid inclusions. Journal of Asian Earth Sciences. 28 (4): 409-422.

[70]. Hezarkhani, A. (2006). Petrology of the intrusive rocks within the Sungun porphyry copper deposit, Azerbaijan, Iran. Journal of Asian Earth Sciences. 27 (3): 326-340.

[71]. Shahabpour, J. (1982). Aspects of alteration and mineralization at the Sar-Cheshmeh copper-molybdenum deposit. Doctoral dissertation, University of Leeds.

[72]. Asadi, S., Moore, F., Zarasvandi, A. and Khosrojerdi, M. (2013). First report on the occurrence of CO2-bearing fluid inclusions in the Meiduk porphyry copper deposit, Iran: implications for mineralisation processes in a continental collision setting. Geologos. 19 (4): 301-320.

[73]. Mortazavi, M., Tahmasebi, P. and Hezarkhani, A. (2010). Element Mobility in Alteration Zones Within Miduk Porphyry Copper Deposit, Shahr–Babak, Kerman, Iran. Australian Journal of Basic and Applied Sciences. 4 (2): 197-207.

[74]. Beane, R.E. and Bodnar, R.J. (1995). Hydrothermal fluids and hydrothermal alteration in porphyry copper deposits. Porphyry copper deposits of the American Cordillera. Arizona Geol Soc Digest. 20: 83-93.

[75]. Gustafson, L.B. and Hunt, J.P. (1975). The porphyry copper deposit at El Salvador, Chile. Economic Geology. 70 (5): 857-912.

[76]. Seedorff, E., Dilles, J.H., Proffett, J.M., Einaudi, M.T., Zurcher, L., Stavast, W.J.A., ... and Barton, M.D. (2005). Porphyry deposits: Characteristics and origin of hypogene features. Economic Geology 100th anniversary volume. 29: 251-298.

[77]. Beane, R.E. and Titley, S.R. (1981). Porphyry copper deposits. Part II. Hydrothermal alteration and mineralization. Economic geology 75th anniversary volume. pp. 235-269.

[78]. Lowell, J.D. and Guilbert, J.M. (1970). Lateral and vertical alteration-mineralization zoning in porphyry ore deposits. Economic Geology. 65 (4): 373-408.

[79]. IGME-INOMRM (Institute for Geological & Mining Exploration & Institution of Nuclear and Other Mineral Raw Materials) (1973). Exploration for ore deposits in Kerman Region. Iran Geological Survey Report No. Yu/53; Iran Geological Survey (Beograd, Yugoslavia). 247 P.

[80]. Taghipour, N., Aftabi, A. and Mathur, R. (2008). Geology and Re-Os Geochronology of Mineralization of the Miduk Porphyry Copper Deposit, Iran. Resource Geology. 58 (2): 143-160.

[81]. Dai, F., Zhou, Q., Lv, Z., Wang, X. and Liu, G. (2014). Spatial prediction of soil organic matter content integrating artificial neural network and ordinary kriging in Tibetan Plateau. Ecological Indicators. 45: 184-194.

[82]. Isaaks, E.H. and Srivastava, R.M. (1989). An Introduction to Applied Geostatistics. Oxford University Press, New York. 561 P.

[83]. Krige, D.G. (1951). A statistical approach to some basic mine valuation problems on the

Witwatersrand. Journal of the Chemical, 6 Metallurgical and Mining Society. 52: 119-139.

[84]. Matheron, G. (1963). Principles of Geostatistics. Economic Geology. 58: 1246-1266.

[85]. Pokhrel, R.M., Kuwano, J. and Tachibana, S. (2013). A kriging method of interpolation used to map liquefaction potential over alluvial ground. Engineering geology. 152: 26-37.

[86]. Hu, H. and Shu, H. (2015). An improved coarse-grained parallel algorithm for computational acceleration of ordinary Kriging interpolation. Computers & Geosciences. 78: 44-52.

[87]. Vann, J. and Guibal, D. (1998). Beyond Ordinary Kriging–An overview of non-linear estimation, Proceedings of a one day symposium: Beyond Ordinary Kriging.

[88]. Goovaerts, P. (1997). Geostatistics for natural resources evaluation. Oxford University Press on Demand.

[89]. Savory, P.J. (2012). Geostatistical methods for estimating iron, silica and alumina grades within the hardcap of the section seven iron deposit. Tom Price.

[90]. Matheron, G. (1971). The theory of regionalized variables and its application. Les Cahiers du Centre de Morphologie mathematique de Fontainbleau, no. 5, Ecole Nationale Superieure des Mines de Paris.

[91]. Kitanidis, P.K. (1997). Introduction to geostatistics: applications in hydrogeology. Cambridge University Press. 65-74 pp.

[92]. Cressie, N.A.C. (1993). Statistics for Spatial Data. Wiley Series in Probability and Mathematical Statistics: Applied Probability and Statistics. New York: John Wiley & Sons, Inc.

[93]. Wackernagel, H. (2003). Multivariate Geostatistics: An Introduction with Applications (3rd ed.). Berlin, Heidelberg: Springer.

[94]. Webster, R. and Oliver, M.A. (2007). Geostatistics for Environmental Scientists (2nd ed.). Statistics in Practice. Chichester: John Wiley & Sons, Ltd. pp. 155-159.

[95]. Samanta, B. and Bandopadhyay, S. (2009). Construction of a radial basis function network using an evolutionary algorithm for grade estimation in a placer gold deposit. Computers & Geosciences. 35 (8): 1592-1602.

[96]. Chatterjee, S., Bhattacherjee, A., Samanta, B. and Pal, S.K. (2006). Ore grade estimation of a limestone deposit in India using an artificial neural network. Applied GIS. 2 (1): 2-1

[97]. Gholamnejad, J., Kasmaee, S., Kohsary, A. and Nezamolhosseini, A. (2012). Grade estimation of ore stockpiles by using Artificial Neural Networks: case study on Choghart Iron Mine in Iran. International Journal of Mining and Mineral Engineering. 4 (1): 17-25.

[98]. Rajasekaran, S. and, Pai, G.V. (2003). Neural networks, fuzzy logic and genetic algorithm: synthesis and applications (with cd). PHI Learning Pvt. Ltd., 441 P.

[99]. Szymczyk, P. and Szymczyk, M. (2015). Classification of geological structure using ground penetrating radar and laplace transform artificial neural networks. Neurocomputing. 148: 354-362.

[100]. Van der Baan, M. and Jutten, C. (2000). Neural networks in geophysical applications. Geophysics. 65 (4): 1032-1047.

[101]. Berger, B.R., Ayuso, R.A., Wynn, J.C. and Seal, R.R. (2008). Preliminary model of porphyry copper deposits. USGS, Open-file Report. 1321 P.

[102]. Soltani, F., Afzal, P. and Asghari, O. (2014). Delineation of alteration zones based on Sequential Gaussian Simulation and concentration–volume fractal modeling in the hypogene zone of Sungun copper deposit, NW Iran. Journal of Geochemical Exploration. 140: 64-76.

[103]. Carranza, E.J.M. (2011). Analysis and mapping of geochemical anomalies using logratiotransformed stream sediment data with censored values. J. Geochem. Explor. 110: 167-185.

مشخص کردن زون‌های دگرسانی بر اساس مدل‌سازی‌های کریجینگ، شبکه‌های عصبی مصنوعی و فرکتالی عیار-حجم در زون هایپوژن نهشته پورفیری مس میدوک، جنوب شرقی ایران

امید غلامپور[۱]، اردشیر هزارخانی[۱*]، عباس مقصودی[۱] و مجید موسوی[۲]

۱- دانشکده مهندسی معدن و متالورژی، دانشگاه صنعتی امیرکبیر، ایران
۲- شرکت بین‌المللی صنایع مس ایران، معدن میدوک، کرمان، ایران

ارسال ۲۰۱۸/۵/۲۶، پذیرش ۲۰۱۸/۷/۲۱

* نویسنده مسئول مکاتبات: ardehez@aut.ac.ir

چکیده:

این پژوهش، روشی کمی را برای مشخص کردن زون‌های دگرسانی در زون هایپوژن نهشته مس پورفیری میدوک (جنوب شرقی ایران) بر اساس داده‌های مغزه‌های حفاری ارائه می‌دهد. مهم‌ترین هدف این کار، استفاده از روش‌های مدل‌سازی کریجینگ معمولی (OK)، شبکه‌های عصبی مصنوعی (ANNs) و فرکتال عیار- حجم (C-V) بر روی داده‌های عیاری مس به منظور جداسازی زون‌های مختلف آلتراسیون بود. ناهمسانگردی بر اساس محاسبه نیم- واریوگرام تجربی داده‌های مس انجام گرفت؛ سپس مهم‌ترین جهت‌های واریوگرافی شناسایی و ارزیابی شدند. در ادامه، مدل بلوکی عیار مس با استفاده از کریجینگ و شبکه‌های عصبی مصنوعی ساخته شد؛ سپس نمودارهای لگاریتمی مدل‌سازی فرکتالی عیار- حجم برای مشخص کردن مقادیر آستانه مس برای شناسایی آلتراسیون‌ها ترسیم شدند. بر اساس همبستگی بین مدل‌های زمین‌شناسی و نتایج حاصل از مدل‌سازی فرکتالی عیار-حجم، مقادیر مس کمتر از ۰/۴۷۹٪ در مدل کریجینگ با صحت کلی (OA) ۰/۸۳ دارای بیشترین همپوشانی با زون دگرسانی فیلیک بود. همبستگی فضایی بین زون دگرسانی پتاسیک در یک مدل سه‌بعدی زمین‌شناسی با زون‌های با عیار بالا در مدل فرکتالی عیار- حجم نشان داد که مقادیر مس بین ۰/۴۷۹٪ و ۱/۰۲۳٪ در مدل کریجینگ بهترین صحت کلی (۰/۷۸) را دارند. در نهایت، فعالیت‌های انجام شده در این پژوهش بر اساس همبستگی بین دسته‌های دو دویی مدل‌های زمین‌شناسی و فرکتال در زون هایپوژن مشخص کرد که مدل‌سازی کریجینگ می‌تواند زون‌های فیلیک (با عیار پایین‌تر) و پتاسیک (با عیار بالاتر) را بهتر از شبکه‌های عصبی مصنوعی مشخص نماید.

کلمات کلیدی: مدل فرکتالی عیار-حجم، کریجینگ معمولی، شبکه‌های عصبی مصنوعی، نهشته مس پورفیری میدوک، زون‌های دگرسانی.